ACS APPLIED MATERIALS & INTERFACES

Research Article

www.acsami.org

Sonochemical Fabrication of Dual-Targeted Redox-Responsive Smart Microcarriers

Zhanfeng Li,[†] Cong Zhang,[†] Bingnan Wang,[†] Hongyan Wang,[†] Xuesi Chen,[‡] Helmoth Möhwald,[§] and Xuejun Cui*[,†]

[†]College of Chemistry, Jilin University, Changchun, 130012, P. R. China

[‡]Key Laboratory of Polymer Ecomaterials, Changchun Institute of Applied Chemistry, Chinese Academy of Sciences, Changchun, 130022, P. R. China

[§]Department of Interfaces, Max Planck Institute of Colloids and Interfaces, D-14424 Potsdam, Germany

ABSTRACT: In the present study, the molecular and magnetic dual-targeted redox-responsive folic acid−cysteine−Fe_3O_4 microcapsules (FA−Cys−Fe_3O_4 MCs) have been synthesized via the sonochemical technique, and targeting molecule (folic acid) and Fe_3O_4 magnetic nanoparticles are introduced into the microcapsule shells successfully. The obtained FA−Cys−Fe_3O_4 MCs show excellent magnetic responsive ability by the oriented motion under an external magnetic field. The hydrophobic fluorescent dye (Coumarin 6) is successfully loaded into the FA−Cys−Fe_3O_4 MCs, demonstrating that it could be also easily realized to encapsulate hydrophobic drugs into the FA−Cys−Fe_3O_4 MCs when the drugs are dispersed into the oil phase before sonication. Cellular uptake demonstrates that FA−Cys−Fe_3O_4 MCs could target selectively the cells via folate-receptor-mediated endocytosis. Moreover, the FA−Cys−Fe_3O_4 MCs show their potential ability to be an attractive carrier for drug controlled release owing to the redox responsiveness of the disulfide in the microcapsule shells.

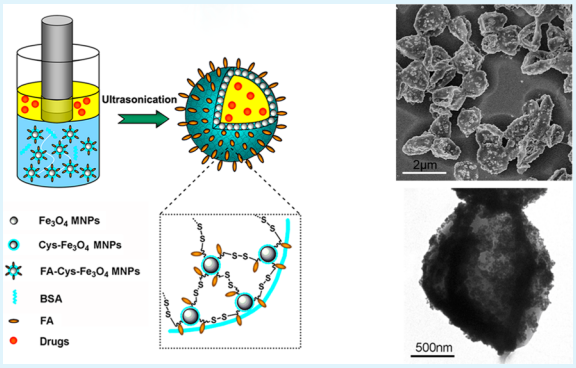

KEYWORDS: *sonochemical, dual-targeted, redox-responsive, microcapsule*

1. INTRODUCTION

Microcapsules are microsize containers with a specific geometric structure for encapsulation of drugs or other materials.[1−3] The biomaterials such as proteins, lipids, and amino acids are good microcapsule materials and have prospective applications in the fields of drug or gene delivery, drug controlled release, and magnetic resonance imaging (MRI).[4−7] In recent years, protein microcapsules or lipid microcapsules have been focused on the treatment of serious diseases (heart disease, cancer, etc.) as effective drug delivery carriers in the biomedical field.

Many efforts have been devoted to prepare biomaterial microcapsules, and various approaches have been developed.[8−14] Suslick and cooperators have developed a new synthesis method for biomaterial microcapsules by using ultrasonic radiation and successfully embedded gas or water-insoluble liquid into protein microcapsules and explored its synthesis mechanism further.[15−17] The sonochemical method has been proven to be simple and efficient owing to its convenient process, simple experimental devices, superior products, and significant saving time in production.[18,19] Moreover, the hydrophobic drugs dispersed in the oil phase can be directly loaded into microcapsules without being destroyed under a high-intensity ultrasound.[20]

It will be very interesting and valuable to introduce targeting material or stimuli-responsive material into the biomaterial microcapsules or immobilize them onto the microcapsule walls, since there are several potential advantages of the targeted stimuli-responsive biomaterial microcapsules. First, microcapsule shells are generally biodegradable due to their biomaterial constituents and the existence of hydrolytic enzymes *in vivo*, and hence, there is little negative effect from the biomaterial microcapsules.[21] Second, a certain amount of hydrophobic drugs can be kept in the biomaterial microcapsules before arriving at the targeted tumor sites or pathological cells, avoiding the side effects of drugs that harm the normal tissues.[22] Third, owing to the existence of targeting material, biomaterial microcapsules can be guided accurately to release the drugs at the specified illness sites. Fourth, on the basis of disulfide bonds, biomaterial microcapsules possess excellent redox responsiveness, which can control release of the drugs when cleavage of disulfide bonds occurs.[23−25] Furthermore, the drug controlled release might help to overcome the multidrug resistance (MDR) of cancer cells.[26−28]

Received: August 26, 2014
Accepted: November 28, 2014
Published: November 28, 2014

Herein, we design a facile sonochemical route for the fabrication of dual-targeted redox-responsive folic acid−cysteine−Fe_3O_4 microcapsules (FA−Cys−Fe_3O_4 MCs) (Scheme 1). Cysteine (Cys) can provide sulfhydryl groups

Scheme 1. Synthesis Schematic of FA−Cys−Fe_3O_4 MNPs (A) and FA−Cys−Fe_3O_4 MCs (B)

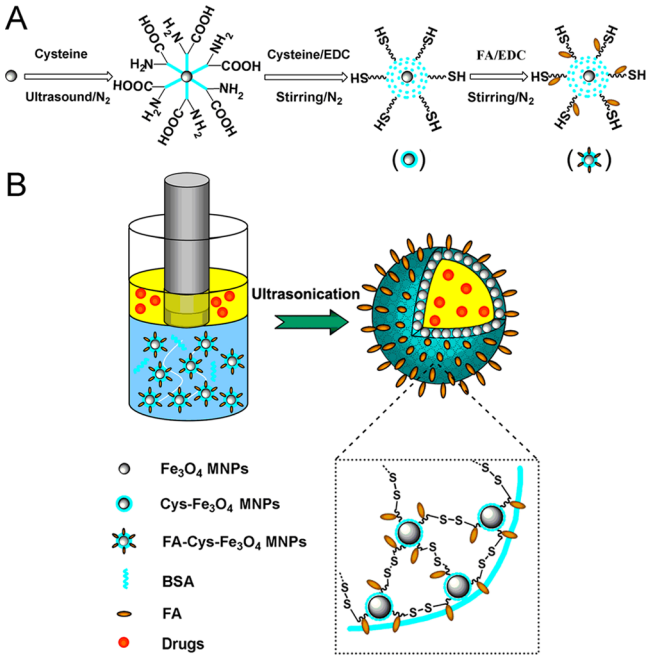

for the formation of disulfide bonds that are necessary for fabricating microcapsules and achieving potential redox responsiveness. Fe_3O_4 magnetic nanoparticles (Fe_3O_4 MNPs) are a therapeutic magnetic material owing to their superparamagnetism, chemical stability, and biocompatibility.[29−31] They are available for the motion and collection of targeted drug carriers through an outer magnetic field, which can guide the transportion of targeted drug carriers to the specified illness sites.[32,33] Folic acid (FA) is a novel targeting molecule and has been found to be a good affinity ligand of the folate receptors (FRs) which have been identified as a cancer marker.[34−36] Introduction of FA can help the microcapsules selectively bind and deliver the drug into the targeted cells via the FA-receptor-mediated endocytosis.[37] In addition, there were abundant reductive agents in the cancer cells, such as glutathione (GSH).[38−40] Once the FA−Cys−Fe_3O_4 MCs were absorbed into the cancer cells by the FR-mediated endocytosis, the reductive agents could cause the disulfide cleavage reactions of the microcapsules and release the drugs instantly.

2. EXPERIMENTAL SECTION

Materials. Ferrous chloride tetrahydrate ($FeCl_2·4H_2O$, >99%) and ferric chloride hexahydrate ($FeCl_3·6H_2O$, >99%) were purchased from Tianjin Guangfu Chemical Reagents Company (Tianjin, China). Aqueous ammonia (NH_4OH, 25%, Beijing Chemical Reagent Company, China), dimethyl sulfoxide (DMSO), *N*,*N*-dimethylformamide (DMF), and sodium citrate ($C_6H_5Na_3O_7$, >99.0%, Beijing Chemical Reagent Company, China) were purchased. Bovine serum albumin (BSA), 1-ethyl-3-(3-dimethylaminepropyl) carbodiimide hydrochloride (EDC), and cysteine (Cys) were purchased from Shanghai Boao Biochemical Technology (Shanghai, China). Folic acid (FA) and Coumarin 6 (C6) were purchased from Sinopharm Chemical Reagent Limited Corporation (Shanghai, China). Phosphate buffer solution (PBS) was prepared by us. All other chemicals were of analytical grade and were used without further purification.

Immobilization of Cys onto the Fe_3O_4 MNPs. The Fe_3O_4 MNPs with an average particle size of 20 nm were synthesized through a chemical coprecipitation method. For the functionalization of Fe_3O_4 MNPs with Cys, 60 mg of Fe_3O_4 MNPs was dispersed into 20 mL of PBS (0.003 M, pH 6.0) and sonicated for 30 min. Then, Cys aqueous solution (20 mg/mL, 3 mL) was injected into the resulting Fe_3O_4 colloidal solution, and sonication of the mixture was vigorously implemented for about 30 min under nitrogen gas (N_2). After that, Cys and EDC in a mole ratio of 1:3 were added into the above-mentioned mixed solution and fast mechanical stirring was carried out in the 20 °C water bath. After 24 h, the composite Cys−Fe_3O_4 magnetic nanoparticles (Cys−Fe_3O_4 MNPs) were collected centrifugally at 12 000 rpm and washed several times with deionized water to remove the unreacted Cys, and then dialyzed against deionized water for 48 h at room temperature. Finally, the Cys−Fe_3O_4 MNPs were obtained via an external magnetic field and redispersed into PBS (0.003 M, pH 6.0).

FA Conjugated Cys−Fe_3O_4 MNPs. FA (10 mg) and EDC (60 mg) were dissolved in DMSO and agitated for 30 min, in which EDC could activate the carboxyl group of FA. Then, the DMSO solution was added into the colloidal solution containing Cys−Fe_3O_4 MNPs (10 mg/mL). After agitating the mixtures under dark conditions for 24 h at room temperature, the supernatant was decanted while the composite FA−Cys−Fe_3O_4 magnetic nanoparticles (FA−Cys−Fe_3O_4 MNPs) were kept in the reaction flask using an external magnet, and the FA−Cys−Fe_3O_4 MNPs were washed several times to remove the free FA and dispersed in deionized water.

Preparation of Dual-Targeted Microcapsules (FA−Cys−Fe_3O_4 MCs). A small amount of BSA (1 wt %, 100 μL) was introduced into the FA−Cys−Fe_3O_4 MNP solution (3 wt %, 4 mL), and silicone oil solution (400 μL) was layered over the BSA and FA−Cys−Fe_3O_4 MNP mixed solution. Then, an ultrasonicator probe (GEX 600, Sonics & Materials, New town, CT, USA) was inserted into the solution. The tip of the ultrasonicator probe should be laid at the oil−water interface and the assembly was maintained in an ice-cooling bath which could control the temperature of the solution below 30 °C during the ultrasound treatment. An acoustic power of 350 $W·cm^{-2}$ was carried out at 20 kHz frequency in 6 min. During the ultrasonication, the oil/water solution became a brown suspension. The resultant suspension was stored at 4 °C, waiting for measurements.

Cellular Uptake of FA−Cys−Fe_3O_4 MCs. To evaluate the cellular uptake of FA−Cys−Fe_3O_4 MCs by means of CLSM and flow cytometry, coumarin 6 (C6) was dispersed in the oil phase and then was loaded into the FA−Cys−Fe_3O_4 MCs by sonication. For the CLSM test, HeLa cells seeded in six-well plates (1×10^5 cells per well) were incubated for 24 h before endocytosis. Some wells were pretreated with FA (10 mg/mL) for 1 h and then replaced with C6-loaded FA−Cys−Fe_3O_4 MCs in serum-free medium (2 mL). The other wells were incubated with C6-loaded FA−Cys−Fe_3O_4 MCs in serum-free medium (2 mL) for 6 h. Afterward, the cells were rinsed with PBS (pH 7.4) and fixed with ethanol (75%). The CLSM analysis was carried out using a confocal laser-scanning microscope. For flow cytometric assay, HeLa cells were seeded in six-well plates (2×10^5 cells per well) and incubated for 24 h. When the cells reached 70−80% confluence, C6-loaded FA−Cys−Fe_3O_4 MCs were added into the wells and incubated for another 6 h. The cells pretreated with FA (10 mg/mL) for 1 h were set as the control. Subsequently, the cells were harvested and resuspended with PBS, and the flow cytometry was determined by a FACS Calibur instrument.

Controlled Release of FA−Cys−Fe_3O_4 MCs. A 3 mL portion of as-synthesized C6-loaded FA−Cys−Fe_3O_4 MC solution was injected into dialysis tubing (3500). Then, the dialysis tubing was immersed into the vessel with the mixed solution of DMF and deionized water (v/v = 1:2) containing DL-dithiothreitol (DTT, 10 mM) and the vessel was vibrated by 150 rpm in the 37 °C water bath. The absorbance of the dialysate was measured by a UV−vis spectrophotometer at different times and the measurements were recorded.

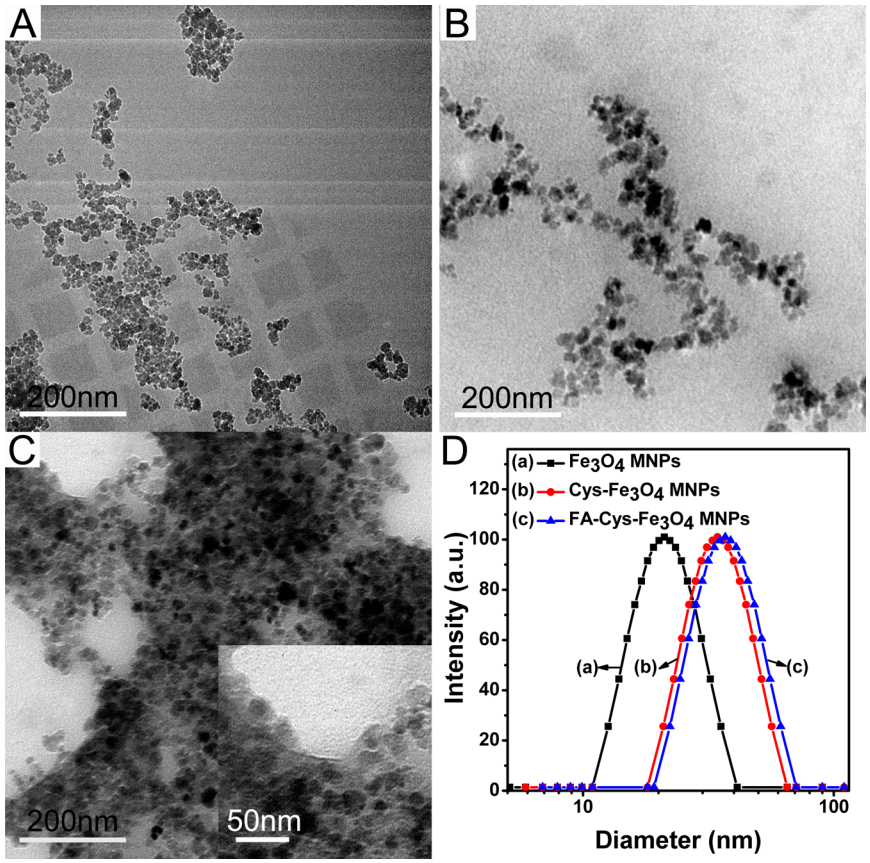

Figure 1. TEM images of Fe_3O_4 MNPs (A), Cys−Fe_3O_4 MNPs (B), and FA−Cys−Fe_3O_4 MNPs (C); the size distribution of Fe_3O_4 MNPs, Cys−Fe_3O_4 MNPs, and FA−Cys−Fe_3O_4 MNPs (D).

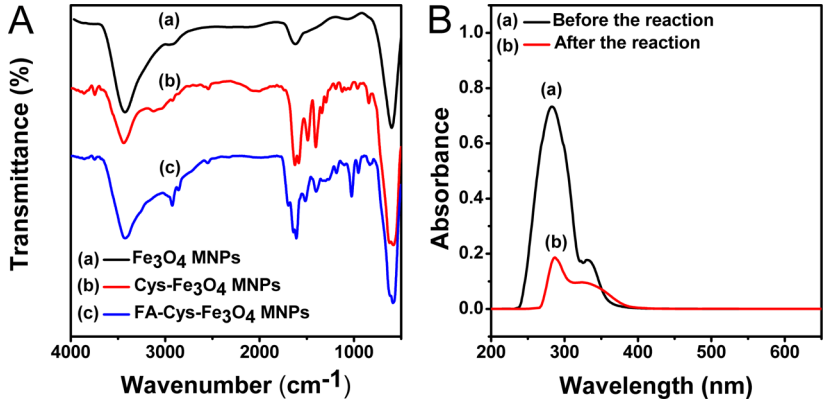

Figure 2. FTIR spectrum of Fe_3O_4 MNPs, Cys−Fe_3O_4 MNPs, and FA−Cys−Fe_3O_4 MNPs (A); UV−vis spectra of the FA solution before and after the reaction of immobilization of FA on the Cys−Fe_3O_4 MNPs (B).

Measurements. Transmission electron microscopy (TEM) images were recorded using the JEOL JEM-2100F transmission microscope at an accelerating voltage of 200 kV. The preparation samples dispersed in water were dropped onto an amorphous carbon-coated copper grid and allowed to air-dry at room temperature. The morphology of samples was investigated using the field emission scanning electron microscope (FESEM) with a Hitachi S-4800 FESEM. Confocal laser scanning microscopy (CLSM) images were taken with a confocal laser-scanning system TCLS attached to an inverse microscope (FV1000) from Olympus (Japan). The flow cytometry was evaluated using a FACS Calibur instrument (BD Bioscience Mountain View, USA). The UV−vis absorption was observed by a UV-2550 spectrophotometer from Shimadzu (Japan). The size distributions of nanoparticles and microcapsules were measured by dynamic light scattering (DLS) with a 90Plus/BI-MAS, and each sample was measured five times. Fourier transform infrared spectra (FTIR) of KBr powder-pressed pellets were recorded in the range 400−4000 cm^{-1} on a Nicolet Instruments Research Series 5PC Fourier Transform Infrared spectrometer.

3. RESULTS AND DISCUSSION

The FA−Cys−Fe_3O_4 MNPs were synthesized through a multi-step process, as shown in Scheme 1A. First, the Fe_3O_4 MNPs were modified with Cys to prepare composite Cys−Fe_3O_4 magnetic nanoparticles (Cys−Fe_3O_4 MNPs).[41−43] Then, FA was immobilized on the composite Cys−Fe_3O_4 MNPs via an EDC-mediated coupling reaction.[44] Eventually, the composite FA−Cys−Fe_3O_4 magnetic nanoparticles (FA−Cys−Fe_3O_4

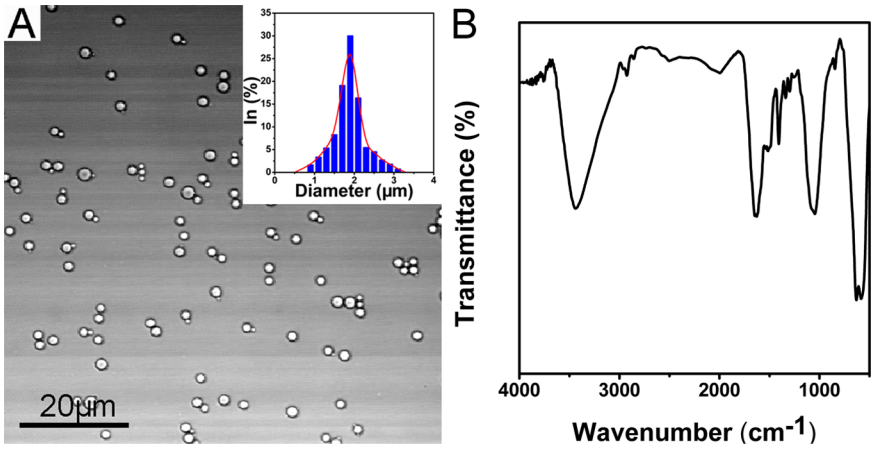

Figure 3. Microscope image and diameter distribution of FA−Cys−Fe_3O_4 MCs whose polydispersity was 0.213 (A); the FTIR spectrum of FA−Cys−Fe_3O_4 MC shells (B).

MNPs) were obtained. TEM images of Fe_3O_4 MNPs, Cys−Fe_3O_4 MNPs, and FA−Cys−Fe_3O_4 MNPs are shown in Figure 1. It could be seen obviously from the inset of Figure 1C that Fe_3O_4 MNPs were embedded in the Cys and FA shells. Meanwhile, it was worth noticing that the diameter of Fe_3O_4 MNPs increased successively after modifying with Cys and immobilization of FA (Figure 1D).

The FTIR spectrum analysis gave us some insights into the components of FA−Cys−Fe_3O_4 MNPs, and the results are shown in Figure 2A. The curves revealed well-defined characteristic adsorption peaks of Cys at 2550 cm^{-1} (ν_{SH}),[45] which was a weak band. The adsorption peaks of 1690 and 1505 cm^{-1} were attributed to vibration adsorption of the carboxyl and phenyl which belonged to FA.[46,47] The characteristic absorption peaks of Fe_3O_4 could be found around 578 cm^{-1}. Obviously, after immobilization of FA onto the Cys−Fe_3O_4 MNPs, there were sulfhydryl groups remaining on the surface of the Fe_3O_4 MNPs. Moreover, the characteristic shoulder around λ = 285 nm in the UV−vis spectrum, as shown in Figure 2B, also confirmed that FA was immobilized onto the Cys−Fe_3O_4 MNP surface successfully.[48−50] In addition, the immobilized amount of FA was quantified by subtracting the UV absorbance of the supernatant solution after the reaction from that of the original solution. Consequently, through the calculation, we could confirm that the reacting density of FA on the Cys−Fe_3O_4 MNP surface was about 40 mg/g.

The dual-targeted redox-responsive microcapsules (FA−Cys−Fe_3O_4 MCs) were fabricated by the sonochemical method as mentioned before (Scheme 1B). The FA−Cys−Fe_3O_4 MCs in the microscope (Figure 3A) showed a spherical morphology with a mean diameter of 1.9 μm which was confirmed by the DLS measurement, as shown in the inset of Figure 3A. Most of the FA−Cys−Fe_3O_4 MCs could be kept stably in the water solution over a month. Additionally, the characteristic absorption peaks of FA could be observed in the FTIR spectrum of the microcapsule shells (Figure 3B), which proved that FA still remained on the microcapsule shells after the ultrasound reaction.

As shown in Figure 4A and B, the SEM images gave us the finer morphology of the FA−Cys−Fe_3O_4 MCs. FA−Cys−Fe_3O_4 MCs were collapsed, and some were creasy due to the elimination of the inner oil phase from the soft microcapsules, and their surfaces were scraggly ascribed to Fe_3O_4 MNPs. Moreover, the compact structure still remained well, indicating

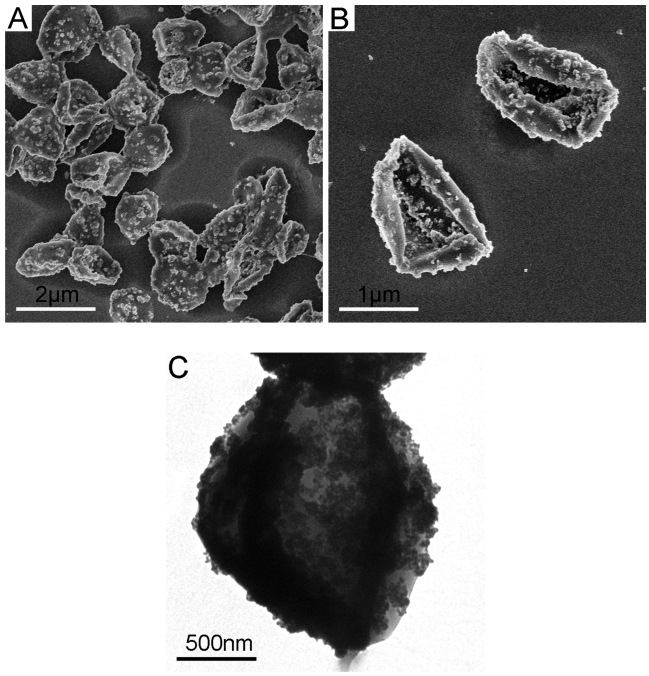

Figure 4. SEM images (A, B) and TEM image (C) of FA−Cys−Fe_3O_4 MCs.

that the FA−Cys−Fe_3O_4 MCs were robust enough to be used as carriers for loading of the hydrophobic material or hydrophobic drugs. The shell structure of FA−Cys−Fe_3O_4 MCs was observed by TEM further (Figure 4C), and it could be clearly seen that the Fe_3O_4 MNPs were embedded evenly in the shells of the FA−Cys−Fe_3O_4 MCs. The formation of the microcapsule shells was attributed to the sulfhydryl groups cross-linking among the Cys layers that were conjugated onto the surface of the Fe_3O_4 MNPs, which was induced by sonication.[51] Owing to Fe_3O_4 MNPs loaded densely into the microcapsule shells, the FA−Cys−Fe_3O_4 MCs promised excellent magnetic responsive properties.

The FA−Cys−Fe_3O_4 MCs possessed a superior magnetic response, which was demonstrated by the motion and collection of the FA−Cys−Fe_3O_4 MCs in an external magnetic field (Figure 5). The initial FA−Cys−Fe_3O_4 MC aqueous dispersion was a nontransparent brown suspension (Figure 5a). When a magnet was placed on one side of the vial, the

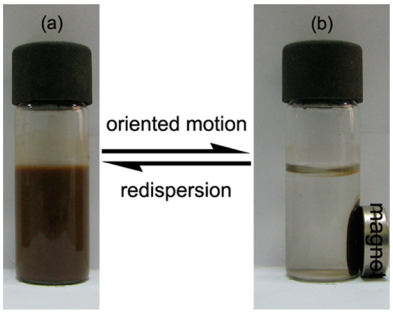

Figure 5. FA−Cys−Fe_3O_4 MCs in aqueous solution (a) and their targeted movement under external magnetic stimuli (b).

suspension would become transparent in a very short time, and the FA−Cys−Fe_3O_4 MCs aggregated onto the side of the vial close to the magnet (Figure 5b). The phenomenon illustrated that the FA−Cys−Fe_3O_4 MCs could be manipulated to move in a desired direction by an external magnet. After removal of the magnet, it was easy to redisperse the FA−Cys−Fe_3O_4 MCs into the water by gentle shaking. While the magnet was close to one side of the vial once more, the FA−Cys−Fe_3O_4 MCs were collected again, demonstrating that the FA−Cys−Fe_3O_4 MCs possessed satisfactory magnetic response and there was little magnetic loss with time owing to the protection of the outermost cross-linked shells. Hence, it could be concluded that the obtained FA−Cys−Fe_3O_4 MCs were possible to be applied in the field of targeted delivery owing to their excellent magnetic responsive properties.[52]

To verify the capacity of hydrophobic drugs encapsulated into the FA−Cys−Fe_3O_4 MCs, hydrophobic dye could be loaded into the FA−Cys−Fe_3O_4 MCs as a substitute for the hydrophobic drugs. The fluorescent dye coumarin 6 (C6) was insoluble in aqueous solution and usually regarded as a model hydrophobic drug,[20,53−55] so we could disperse C6 in the oil phase and loaded it into the FA−Cys−Fe_3O_4 MCs by sonication. The C6-loaded FA−Cys−Fe_3O_4 MCs were indistinctive in the transmission mode (Figure 6A), while the

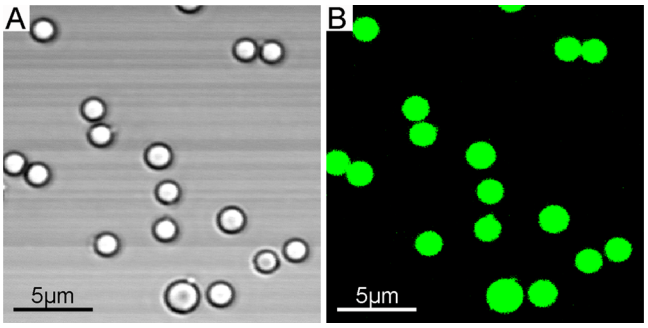

Figure 6. Confocal microscope images of C6-loaded FA−Cys−Fe_3O_4 MCs in transmission mode (A) and fluorescence mode (B).

signals of green fluorescence could be observed clearly in the fluorescence mode (Figure 6B). The signals were originating from C6 motivated by the laser. Superimposing the transmission mode and the fluorescence mode, we could observe clearly that the signals were originated from the interior of FA−Cys−Fe_3O_4 MCs, which demonstrated that the hydrophobic C6 was encapsulated successfully into the FA−Cys−Fe_3O_4 MCs. Meanwhile, there were few fluorescent signals in the solution or out of the microcapsules, proving that there was little leakage of C6 from the FA−Cys−Fe_3O_4 MCs owing to the protection of the tough microcapsule shells.[56] Accordingly, the as-synthesized FA−Cys−Fe_3O_4 MCs could be excellent carriers for targeted delivery, especially for hydrophobic anticancer drugs (i.e., taxol, camptothecin, etc.) or other hydrophobic materials.

FRs were overexpressed in more than 90% of the ovarian carcinomas as a highly selective tumor marker,[57,58] so HeLa cells with FRs were selected to monitor FA-mediated internalization of C6-loaded FA−Cys−Fe_3O_4 MCs through the CLSM.[59] As Figure 7A shows, a quite strong green fluorescence was observed in the HeLa cells after incubation, mainly in the intracellular regions, indicating that C6-loaded FA−Cys−Fe_3O_4 could realize the endocytosis with high efficiency. To evaluate the mechanism of cellular uptake clearly, we pretreated HeLa cells with FA (10 mg/mL) for 1 h before the incubation of C6-loaded FA−Cys−Fe_3O_4 MCs to block FRs. The intracellular fluorescent intensity of HeLa cells was remarkably weakened (Figure 7B), indicating that the cellular uptake of C6-loaded FA−Cys−Fe_3O_4 MCs was reduced by free FA in the pretreatment. The data suggested that the internalization of C6-loaded FA−Cys−Fe_3O_4 MCs into cells was induced by a FA-dependent pathway.

To get further insight into the mechanism for cellular uptake, the cellular internalization of C6-loaded FA−Cys−Fe_3O_4 MCs was investigated through flow cytometry. When HeLa cells were pretreated with FA (10 mg/mL) for 1 h, the internalization of C6-loaded FA−Cys−Fe_3O_4 MCs into cells was apparently inhibited with a lower fluorescence intensity observed (from b to c, Figure 7C). These results were consistent with those in CLSM, demonstrating that the pretreatment of FA could significantly lower the cellular uptake of C6-loaded FA−Cys−Fe_3O_4 MCs and FA−Cys−Fe_3O_4 MCs could target selectively the cells via FR-mediated endocytosis.

The efforts were devoted to confirm whether the FA−Cys−Fe_3O_4 MCs possessed stimuli-sensitive properties for drug controlled release. Owing to the disulfide linkage, the FA−Cys−Fe_3O_4 MCs might be disassembled in the presence of some reductive agents, such as DTT and glutathione.[60,61] Hence, a few disassembly experiments were carried out to demonstrate the redox responsiveness of the microcapsules by addition of DTT. To test the dependence of disassembly, C6-loaded microcapsules were treated with DTT (10 mM) and the dye release amount with the time was recorded by a UV−vis spectrophotometer. A direct signal that was diagnostic of C6 release was the absorbance intensity change of C6 in the dialysate. Figure 8 showed the time-dependent absorbance of C6 at the maximum absorption wavelength (λ = 457 nm). When there was no DTT, the absorbance intensity of the dialysate increased relatively slowly throughout the time. In contrast, in the presence of DTT, the release of C6 was accelerated and the absorbance intensity of the dialysate increased obviously with the time. The results suggested that the disassembly of microcapsule structure could be mainly attributed to the cleavage of disulfide bonds and the FA−Cys−Fe_3O_4 MCs had excellent redox-responsive ability for drug controlled release.

CONCLUSION

In summary, we have rationally designed a facile approach for the fabrication of molecular and magnetic dual-targeted redox-responsive FA−Cys−Fe_3O_4 MCs via the sonochemical technique, and targeting molecule (FA) and Fe_3O_4 MNPs

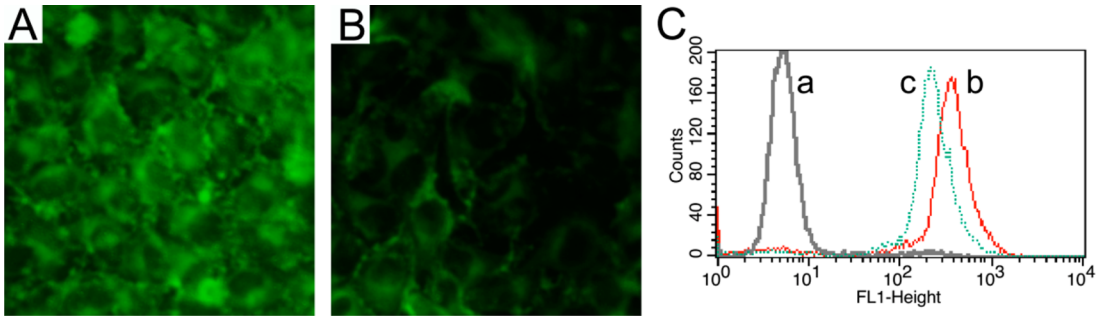

Figure 7. CLSM images of HeLa cells exposed to C6-loaded FA−Cys−Fe_3O_4 MCs (A) and HeLa cells with the pretreatment of FA before being exposed to C6-loaded FA−Cys−Fe_3O_4 MCs (B); flow cytometric analysis of the cellular uptake (C): (a) the control, (b) C6-loaded FA−Cys−Fe_3O_4 MCs, and (c) C6-loaded FA−Cys−Fe_3O_4 MCs after the pretreatment of FA.

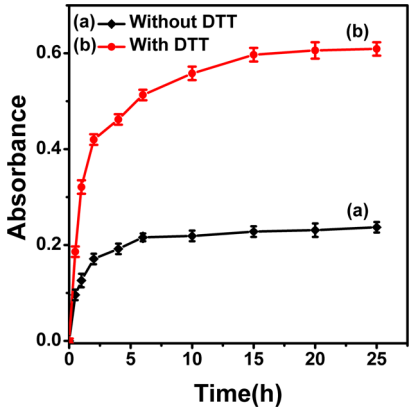

Figure 8. Time-dependent absorbance of C6 in the dialysate without DTT (a) and with DTT (b).

were introduced into the microcapsule shells successfully. The FA−Cys−Fe_3O_4 MCs showed excellent magnetic responsive ability and could be readily moved and collected with the help of an external magnetic field. The hydrophobic fluorescent dye (C6) was loaded successfully into the FA−Cys−Fe_3O_4 MCs, demonstrating that it could be easily realized to encapsulate the hydrophobic drugs into the microcapsules when the drugs were dispersed into the oil phase. Cellular uptake of C6-loaded FA−Cys−Fe_3O_4 MCs demonstrates that FA−Cys−Fe_3O_4 MCs could target selectively the cells via FR-mediated endocytosis. Furthermore, the FA−Cys−Fe_3O_4 MCs showed their potential ability to be an attractive carrier for drug controlled release owing to the redox responsiveness of the disulfide in the microcapsule shells. Besides, the FA−Cys−Fe_3O_4 MCs could be endowed with desired multifunctionality by modifying some functional groups or small molecules on the shells. Accordingly, the dual-targeted redox-responsive FA−Cys−Fe_3O_4 MCs should be excellent candidates as smart carriers for drug targeted delivery and drug controlled release.

AUTHOR INFORMATION

Corresponding Author

*E-mail: cui_xj@jlu.edu.cn.

Notes

The authors declare no competing financial interest.

ACKNOWLEDGMENTS

This work was supported by the National Natural Science Foundation of China (Nos. 21104023 and 21106052) and the Key Program of the Science and Technology Department of Jilin Province, PR China (No. 20140204053GX). Thanks for the help of Dr. Quanshun Li on the cellular experiments.1

REFERENCES

(1) Cavalieri, F.; Micheli, L.; Kaliappan, S.; Teo, B. M.; Zhou, M.; Palleschi, G.; Ashokkumar, M. Antimicrobial and Biosensing Ultrasound-Responsive Lysozyme-Shelled Microbubbles. *ACS Appl. Mater. Interfaces* **2013**, *5*, 464−471.

(2) Pretzl, M.; Neubauer, M.; Tekaat, M.; Kunert, C.; Kuttner, C.; Leon, G.; Berthier, D.; Erni, P.; Ouali, L.; Fery, A. Formation and Mechanical Characterization of Aminoplast Core/Shell Microcapsules. *ACS Appl. Mater. Interfaces* **2012**, *4*, 2940−2948.

(3) Datta, S. S.; Abbaspourrad, A.; Amstad, E.; Fan, J.; Kim, S.; Romanowsky, M.; Shum, H. C.; Sun, B.; Utada, A. S.; Windbergs, M.; Zhou, S.; Weitz, D. A. 25th Anniversary Article: Double Emulsion Templated Solid Microcapsules: Mechanics And Controlled Release. *Adv. Mater.* **2014**, *26*, 2205−2218.

(4) Gedanken, A. Preparation and Properties of Proteinaceous Microspheres Made Sonochemically. *Chem.—Eur. J.* **2008**, *14*, 3840−3853.

(5) Poehlmann, M.; Grishenkov, D.; Kothapalli, S. V. V. N.; Härmark, J.; Hebert, H.; Philipp, A.; Hoeller, R.; Seuss, M.; Kuttner, C.; Margheritelli, S.; Paradossi, G.; Fery, A. On the Interplay of Shell Structure with Low- and High-Frequency Mechanics of Multifunctional Magnetic Microbubbles. *Soft Matter* **2014**, No. 10, 214−226.

(6) Palankar, R.; Pinchasik, B. E.; Schmidt, S.; Geest, B. G. D.; Fery, A.; Möhwald, H.; Skirtach, A. G.; Delcea, M. Mechanical Strength and Intracellular Uptake of $CaCO_3$-Templated LbL Capsules Composed of Biodegradable Polyelectrolytes: the Influence of the Number of Layers. *J. Mater. Chem. B* **2013**, *1*, 1175−1181.

(7) He, Q.; Cui, Y.; Li, J. Molecular Assembly and Application of Biomimetic Microcapsules. *Chem. Soc. Rev.* **2009**, *38*, 2292−2303.

(8) Wu, Z.; Wu, Y.; He, W.; Lin, X.; Sun, J.; He, Q. Self-Propelled Polymer-Based Multilayer Nanorockets for Transportation and Drug Release. *Angew. Chem., Int. Ed.* **2013**, *52*, 7000−7003.

(9) An, Z.; Lu, G.; Möhwald, H.; Li, J. Self-Assembly of Human Serum Albumin (HSA) and l-α-Dimyristoylphosphatidic Acid (DMPA) Microcapsules for Controlled Drug Release. *Chem.—Eur. J.* **2004**, *10*, 5848−5852.

(10) Lu, G.; An, Z.; Tao, C.; Li, J. Microcapsule Assembly of Human Serum Albumin at the Liquid/Liquid Interface by the Pendent Drop Technique. *Langmuir* **2004**, *20*, 8401−8403.

(11) Jeong, W. C.; Kim, S. H.; Yang, S. M. Photothermal Control of Membrane Permeability of Microcapsules for On-Demand Release. *ACS Appl. Mater. Interfaces* **2014**, *6*, 826−832.

(12) Wu, Y.; Lin, X.; Wu, Z.; Möhwald, H.; He, Q. Self-Propelled Polymer Multilayer Janus Capsules for Effective Drug Delivery and Light-Triggered Release. *ACS Appl. Mater. Interfaces* **2014**, *6*, 10476−10481.

(13) Qi, W.; Yan, X.; Duan, L.; Cui, Y.; Yang, Y.; Li, J. Glucose-Sensitive Microcapsules from Glutaraldehyde Cross-Linked Hemoglobin and Glucose Oxidase. *Biomacromolecules* **2009**, *10*, 1212−1216.

(14) Shimanovich, U.; Bernardes, G. J. L.; Knowles, T. P. J.; Cavaco-Paulo, A. Protein Micro- and Nano-Capsules for Biomedical Applications. *Chem. Soc. Rev.* **2014**, *43*, 1361−1371.
(15) Suslick, K. S.; Grinstaff, M. W. Protein Microencapsulation of Nonaqueous Liquids. *J. Am. Chem. Soc.* **1990**, *112*, 7807−7809.
(16) Flannigan, D. J.; Suslick, K. S. Plasma Formation and Temperature Measurement during Single-Bubble Cavitation. *Nature* **2005**, *434*, 52−55.
(17) Angel, U.; Matas, D.; Michaeli, S.; Cavaco-Paulo, A.; Gedanken, A. Microspheres of Mixed Proteins. *Chem.—Eur. J.* **2010**, *16*, 2108−2114.
(18) Wu, J.; Zhu, Y. J.; Cao, S. W.; Chen, F. Hierachically Nanostructured Mesoporous Spheres of Calcium Silicate Hydrate: Surfactant-Free Sonochemical Synthesis and Drug-Delivery System with Ultrahigh Drug-Loading Capacity. *Adv. Mater.* **2010**, *22*, 749−753.
(19) Shimanovich, U.; Perelshtein, I.; Cavaco-Paulo, A.; Gedanken, A. Releasing Dye Encapsulated in Proteinaceous Microspheres on Conductive Fabrics by Electric Current. *ACS Appl. Mater. Interfaces* **2012**, *4*, 2926−2930.
(20) Han, Y.; Shchukin, D.; Yang, J.; Simon, C. R.; Möhwald, H. Biocompatible Protein Nanocontainers for Controlled Drugs Release. *ACS Nano* **2010**, *4*, 2838−2844.
(21) Hu, S. H.; Liu, T. Y.; Liu, D. M.; Chen, S. Y. Nano-Ferrosponges for Controlled Drug Release. *J. Controlled Release* **2007**, *121*, 181−189.
(22) Cui, X.; Li, Z.; Zhong, S.; Wang, B.; Han, Y.; Wang, H.; Möhwald, H. A Facile Sonochemical Route for the Fabrication of Magnetic Protein Microcapsules for Targeted Delivery. *Chem.—Eur. J.* **2013**, *19*, 9485−9488.
(23) Gao, L.; Fei, J.; Zhao, J.; Cui, W.; Cui, Y.; Li, J. pH-and Redox-Responsive Polysaccharide-Based Microcapsules with Autofluorescence for Biomedical Applications. *Chem.—Eur. J.* **2012**, *18*, 3185−3192.
(24) Zhao, J.; Liu, J.; Xu, S.; Zhou, J.; Han, S.; Deng, L.; Zhang, J.; Liu, J.; Meng, A.; Dong, A. Graft Copolymer Nanoparticles with pH and Reduction Dual-Induced Disassemblable Property for Enhanced Intracellular Curcumin Release. *ACS Appl. Mater. Interfaces* **2013**, *5*, 13216−13226.
(25) Cui, Y.; Dong, H.; Cai, X.; Wang, D.; Li, Y. Mesoporous Silica Nanoparticles Capped with Disulfide-Linked PEG Gatekeepers for Glutathione-Mediated Controlled Release. *ACS Appl. Mater. Interfaces* **2012**, *4*, 3177−3183.
(26) Vivek, R.; Thangam, R.; NipunBabu, V.; Rejeeth, C.; Sivasubramanian, S.; Gunasekaran, P.; Muthuchelian, K.; Kannan, S. Multifunctional HER2-Antibody Conjugated Polymeric Nanocarrier-Based Drug Delivery System for Multi-Drug-Resistant Breast Cancer Therapy. *ACS Appl. Mater. Interfaces* **2014**, *6*, 6469−6480.
(27) Kelley, E. G.; Albert, J. N. L.; Sullivan, M. O.; Epps, T. H., III. Stimuli-Responsive Copolymer Solution and Surface Assemblies for Biomedical Applications. *Chem. Soc. Rev.* **2013**, *42*, 7057−7071.
(28) Chen, S.; Ruan, Y.; Brown, J. D.; Gallucci, J.; Maslak, V.; Hadad, C. M.; Badjic, J. D. Assembly of Amphiphilic Baskets into Stimuli-Responsive Vesicles. Developing a Strategy for the Detection of Organophosphorus Chemical Nerve Agents. *J. Am. Chem. Soc.* **2013**, *135*, 14964−14967.
(29) Zeng, T.; Zhang, X.; Wang, S.; Ma, Y.; Niu, H.; Cai, Y. Assembly of a Nanoreactor System with Confined Magnetite Core and Shell for Enhanced Fenton-Like Catalysis. *Chem.—Eur. J.* **2014**, *20*, 6474−6481.
(30) Qiu, Y.; Palankar, R.; Echeverría, M.; Medvedev, N.; Moya, S. E.; Delcea, M. Design of Hybrid Multimodal Poly (Lactic-Co-Glycolic Acid) Polymer Nanoparticles for Neutrophil Labeling, Imaging and Tracking. *Nanoscale* **2013**, *5*, 12624−12632.
(31) Mukhopadhyay, A.; Joshi, N.; Chattopadhyay, K.; De, G. A Facile Synthesis of PEG-Coated Magnetite (Fe_3O_4) Nanoparticles and Their Prevention of the Reduction of Cytochrome C. *ACS Appl. Mater. Interfaces* **2012**, *4*, 142−149.
(32) Tziveleka, L. A.; Bilalis, P.; Chatzipavlidis, A.; Boukos, N.; Kordas, G. Development of Multiple Stimuli Responsive Magnetic Polymer Nanocontainers as Efficient Drug Delivery Systems. *Macromol. Biosci.* **2014**, *14*, 131−141.
(33) McBride, A. A.; Price, D. N.; Lamoureux, L. R.; Elmaoued, A. A.; Vargas, J. M.; Adolphi, N. L.; Muttil, P. Preparation and Characterization of Novel Magnetic Nano-in-Microparticles for Site-Specific Pulmonary Drug Delivery. *Mol. Pharmaceutics* **2013**, *10*, 3574−3581.
(34) Yang, X.; Grailer, J. J.; Pilla, S.; Steeber, D. A.; Gong, S. Tumor-Targeting, pH-Responsive, and Stable Unimolecular Micelles as Drug Nanocarriers for Targeted Cancer Therapy. *Bioconjugate Chem.* **2010**, *21*, 496−504.
(35) Yoo, M. K.; Park, I. K.; Lim, H. T.; Lee, S. J.; Jiang, H. L.; Kim, Y. K.; Choi, Y. J.; Cho, M. H.; Cho, C. S. Folate-PEG-Superparamagnetic Iron Oxide Nanoparticles for Lung Cancer Imaging. *Acta Biomater.* **2012**, *8*, 3005−3013.
(36) Zhou, Y.; Wang, H.; Wang, C.; Li, Y.; Lu, W.; Chen, S.; Luo, J.; Jiang, Y.; Chen, J. Receptor-Mediated, Tumor-Targeted Gene Delivery Using Folate-Terminated Polyrotaxanes. *Mol. Pharmaceutics* **2012**, *9*, 1067−1076.
(37) Lu, T.; Sun, J.; Chen, X.; Zhang, P.; Jing, X. Folate-Conjugated Micelles and Their Folate-Receptor-Mediated Endocytosis. *Macromol. Biosci.* **2009**, *9*, 1059−1068.
(38) Liu, J.; Pang, Y.; Huang, W.; Huang, X.; Meng, L.; Zhu, X.; Zhou, Y.; Yan, D. Redox-Responsive Polyphosphate Nanosized Assemblies: a Smart Drug Delivery Platform for Cancer Therapy. *Biomacromolecules* **2011**, *12*, 1567−1577.
(39) Wen, H. Y.; Dong, H. Q.; Xie, W. J.; Li, Y. Y.; Wang, K.; Pauletti, G. M.; Shi, D. L. Rapidly Disassembling Nanomicelles with Disulfide-Linked PEG Shells for Glutathione-Mediated Intracellular Drug Delivery. *Chem. Commun.* **2011**, *47*, 3550−3552.
(40) Wang, Y. C.; Li, Y.; Sun, T. M.; Xiong, M. H.; Wu, J.; Yang, Y. Y.; Wang, J. Core-Shell-Corona Micelle Stabilized by Reversible Cross-Linkage for Intracellular Drug Delivery. *Macromol. Rapid Commun.* **2010**, *31*, 1201−1206.
(41) Cohen, H.; Gedanken, A.; Zhong, Z. One-Step Synthesis and Characterization of Ultrastable and Amorphous Fe_3O_4 Colloids Capped with Cysteine Molecules. *J. Phys. Chem. C* **2008**, *112*, 15429−15438.
(42) Wang, Y.; Shen, Y.; Xie, A.; Li, S.; Wang, X.; Cai, Y. A Simple Method to Construct Bifunctional Fe_3O_4/Au Hybrid Nanostructures and Tune Their Optical Properties in the Near-Infrared Region. *J. Phys. Chem. C* **2010**, *114*, 4297−4301.
(43) Cao, S. W.; Fang, J.; Shahjamali, M. M.; Wang, Z.; Yin, Z.; Yang, Y.; Boey, F. Y. C.; Barber, J.; Loo, S. C. J.; Xue, C. In Situ Growth of Au Nanoparticles on Fe_2O_3 Nanocrystals for Catalytic Applications. *CrystEngComm* **2012**, *14*, 7229−7235.
(44) Zhao, Z.; Huang, D.; Yin, Z.; Chi, X.; Wang, X.; Gao, J. Magnetite Nanoparticles as Smart Carriers to Manipulate the Cytotoxicity of Anticancer Drugs: Magnetic Control and pH-Responsive Release. *J. Mater. Chem.* **2012**, *22*, 15717−15725.
(45) Sahoo, B.; Devi, K. S. P.; Banerjee, R.; Maiti, T. K.; Pramanik, P.; Dhara, D. Thermal and pH Responsive Polymer-Tethered Multifunctional Magnetic Nanoparticles for Targeted Delivery of Anticancer Drug. *ACS Appl. Mater. Interfaces* **2013**, *5*, 3884−3893.
(46) Du, P.; Zeng, J.; Mu, B.; Liu, P. Biocompatible Magnetic and Molecular Dual-Targeting Polyelectrolyte Hybrid Hollow Microspheres for Controlled Drug Release. *Mol. Pharmaceutics* **2013**, *10*, 1705−1715.
(47) Dong, S.; Cho, H. J.; Lee, Y. W.; Roman, M. Synthesis and Cellular Uptake of Folic Acid-Conjugated Cellulose Nanocrystals for Cancer Targeting. *Biomacromolecules* **2014**, *15*, 1560−1567.
(48) Cheng, D.; Hong, G.; Wang, W.; Yuan, R.; Ai, H.; Shen, J.; Liang, B.; Gao, J.; Shuai, X. Nonclustered Magnetite Nanoparticle Encapsulated Biodegradable Polymeric Micelles With Enhanced Properties for in Vivo Tumor Imaging. *J. Mater. Chem.* **2011**, *21*, 4796−4804.
(49) Mahajan, S.; Koul, V.; Choudhary, V.; Shishodia, G.; Bharti, A. C. Preparation and in Vitro Evaluation of Folate-Receptor-Targeted SPION-Polymer Micelle Hybrids for MRI Contrast Enhancement in Cancer Imaging. *Nanotechnology* **2013**, *24*, 015603−015614.

(50) Wang, F.; Pauletti, G. M.; Wang, J.; Zhang, J.; Ewing, R. C.; Wang, Y.; Shi, D. Dual Surface-Functionalized Janus Nanocomposites of Polystyrene/Fe_3O_4@ SiO_2 for Simultaneous Tumor Cell Targeting and Stimulus-Induced Drug Release. *Adv. Mater.* **2013**, *25*, 3485−3489.
(51) Grinstaff, M. W.; Suslick, K. S. Air-Filled Proteinaceous Microbubbles: Synthesis of an Echo-Contrast Agent. *Proc. Natl. Acad. Sci. U.S.A.* **1991**, *88*, 7708−7710.
(52) Pavlov, A. M.; Geest, B. G. D.; Louage, B.; Lybaert, L.; Koker, S. D.; Koudelka, Z.; Sapelkin, A.; Sukhorukov, G. B. Magnetically Engineered Microcapsules as Intracellular Anchors for Remote Control Over Cellular Mobility. *Adv. Mater.* **2013**, *25*, 6945−6950.
(53) Zhou, L.; He, B.; Huang, J. One-Step Synthesis of Robust Amine- and Vinyl-Capped Magnetic Iron Oxide Nanoparticles for Polymer Grafting, Dye Adsorption, and Catalysis. *ACS Appl. Mater. Interfaces* **2013**, *5*, 8678−8685.
(54) Corrent, S.; Hahn, P.; Pohlers, G.; Connolly, T. J.; Scaiano, J. C.; Fornes, V.; Garc, H. Photochemistry, I. Intrazeolite photochemistry. 22. Acid-Base Properties of Coumarin 6. Characterization in Solution, the Solid State, and Incorporated into Supramolecular Systems. *J. Phys. Chem. B* **1998**, *102*, 5852−5858.
(55) Mulder, C. L.; Reusswig, P. D.; Beyler, A. P.; Kim, H.; Rotschild, C.; Baldo, M. A. Dye Alignment in Luminescent Solar Concentrators: II. Horizontal Alignment for Energy Harvesting in Linear Polarizers. *Opt. Express* **2010**, *18*, 91−99.
(56) Han, Y.; Radziuk, D.; Shchukin, D.; Möhwald, H. Sonochemical Synthesis of Magnetic Protein Container for Targeted Delivery. *Macromol. Rapid Commun.* **2008**, *29*, 1203−1207.
(57) Hu, S. H.; Chen, Y. W.; Hung, W. T.; Chen, I. W.; Chen, S. Y. Quantum-Dot-Tagged Reduced Graphene Oxide Nanocomposites for Bright Fluorescence Bioimaging and Photothermal Therapy Monitored In Situ. *Adv. Mater.* **2012**, *24*, 1748−1754.
(58) Sudimack, J.; Lee, R. J. Targeted Drug Delivery via the Folate Receptor. *Adv. Drug Delivery Rev.* **2000**, *41*, 147−162.
(59) Hu, C.; Liu, Y.; Qin, J.; Nie, G.; Lei, B.; Xiao, Y.; Zheng, M.; Rong, J. Fabrication of Reduced Graphene Oxide and Sliver Nanoparticle Hybrids for Raman Detection of Absorbed Folic Acid: A Potential Cancer Diagnostic Probe. *ACS Appl. Mater. Interfaces* **2013**, *5*, 4760−4768.
(60) Lee, M. H.; Yang, Z.; Lim, C. W.; Lee, Y. H.; Dongbang, S.; Kang, C.; Kim, J. S. Disulfide-Cleavage-Triggered Chemosensors and Their Biological Applications. *Chem. Rev.* **2013**, *113*, 5071−5109.
(61) Lee, M. H.; Kim, J. Y.; Han, J. H.; Bhuniya, S.; Sessler, J. L.; Kang, C.; Kim, J. S. Direct Fluorescence Monitoring of the Delivery and Cellular Uptake of a Cancer-Targeted RGD Peptide-Appended Naphthalimide Theragnostic Prodrug. *J. Am. Chem. Soc.* **2012**, *134*, 12668−12674.